Using quantitative MRI to track cerebral damage in multiple sclerosis: a longitudinal study

Nora Vandeleene[a], Camille Guillemin[a,b], Solène Dauby[a,c], Florence Requier[a,b], Maëlle Charonitis[a,b], Daphne Chylinski[a,b], Evelyne Balteau[a], Pierre Maquet[a,c], Emilie Lommers[a,c*], Christophe Phillips[a,d*]

[a] GIGA CRC in vivo Imaging, University of Liège, Liège, Belgium
[b] Psychology and Cognitive Neuroscience Research Unit, University of Liège, Liège, Belgium
[c] Clinical Neuroimmunology Unit, Neurology Department, CHU Liège, Belgium
[d] GIGA in silico Medicine, University of Liège, Liège, Belgium

* These authors equally contributed to the work.

Corresponding author: Christophe PHILLIPS
GIGA – CRC in vivo imaging B30
Allée du 6 août
4000 Liège
Belgium

Word count:
Main text: 2685; Methods: 2367 (Total: 5052); Abstract: 320

Abbreviations:
ARoC: Annual Rate of Change, **BPF**: Brain Parenchymal Fraction, **CDP**: Confirmed Disability Progression, **cMRI**: Conventional Magnetic Resonance Imaging, **CNS:** Central Nervous System, **GMF**: Grey Matter Fraction, **GLMM**: General Linear Mixed Model, **LF**: Lesion Fraction, **MPM**: Multiparameter mapping, **MRI**: Magnetic Resonance Imaging, **MS**: Multiple Sclerosis, **MT**: Magnetization Transfer, **MTR**: Magnetization Transfer Ratio, **MTsat**: Saturated Magnetization Transfer, **NABT**: Normal Appearing Brain Tissue, **NACGM**: Normal Appearing Cortical Grey Matter, **NADGM**: Normal Appearing Deep Grey matter, **NAWM**: Normal Appearing White Matter, **NEDA-3**: No Evidence of Disease Activity, **RRMS**: Relapsing-Remitting Multiple Sclerosis, **PD**: Proton Density, **PMS**: Progressive Multiple Sclerosis, **qMRI**: Quantitative Magnetic Resonance Imaging, **R1**: Longitudinal Relaxation Rate (1/T1), **R2***: Transverse Relaxation Rate (1/T2*), **TIV**: Total Intracranial Volume, **TPM**: Tissue Probability Map, **US:** Unified Segmentation, **USwL**: Unified Segmentation with Lesion

Abstract

Objectives:

Contrary to conventional MRI (cMRI), quantitative MRI (qMRI) quantifies tissue physical microstructural properties and improves the characterization of cerebral damages in relation with various neurological diseases. With a multi-parameter mapping (MPM) protocol, 4 parameter maps are constructed: saturated magnetization transfer (MTsat), proton density (PD), longitudinal relaxation (R1) and effective transverse relaxation (R2*) rates, reflecting tissue physical properties associated with iron and myelin contents. Here, we used qMRI to investigate the microstructural changes happening over time in multiple sclerosis (MS).

Methods:

Seventeen MS patients (age 25-65, 11 RRMS) were scanned on a 3T MRI, with at least one year separation between two acquisition sessions, and the evolution of their parameters was evaluated within several tissue classes: normal appearing white matter (NAWM), normal appearing cortical and deep gray matter (NACGM and NADGM) as well as focal white matter (WM) lesions. Brain tissue segmentation was performed using US-with-Lesion, an adapted version of the Unified Segmentation (US) algorithm accounting for the lesion tissue class, based on qMRI and FLAIR images. An individual annual rate of change for each qMRI parameter was computed, and its correlation to clinical status was evaluated. As for WM plaques, three areas were defined within them. A Generalized Linear Mixed Model (GLMM) tested the effect of area and time points, as well as their interaction on each median qMRI parameter value.

Results:

Patients with a better clinical evolution showed positive annual rate of change in MT and R2* within NAWM and NACGM, suggesting repair mechanisms in terms of increased myelin content and/or axonal density. When examining focal WM lesions, qMRI parameters within surrounding NAWM showed modification in terms of reduction in MT, R1 and R2* combined with increased of PD even before any focal lesion is visible on conventional FLAIR MRI.

Conclusion:

The results illustrate the benefit of multiple qMRI data in monitoring subtle changes within normal appearing brain tissues and plaque dynamics in relation with tissue repair or disease progression.

Keywords:

Quantitative MRI, relaxometry, longitudinal analysis, multiple sclerosis.

1. Introduction

Multiple sclerosis (MS) is a chronic autoimmune disease of the central nervous system (CNS). The course of the disease may reflect the expression of two clinical phenomena, relapses of acute neurological symptoms followed by partial or complete recovery (remission), and progression, which refers to the steady and irreversible worsening of the clinical status. Relapses are mainly the expression of acute, focal, disseminated and recurrent inflammation occurring within the CNS (i.e., plaques). Plaques are the pathological hallmark of MS and harbor variable degrees of inflammation, demyelination, gliosis and axonal injury [1, 2]. Plaques are not restricted to the white matter (WM), but are also present in the cortex and deep grey matter (GM) [3-5]. The progressive accumulation of disability principally correlates with the early, diffuse and chronic inflammation within the normal appearing white matter (NAWM) and grey matter (NAGM) that is ultimately responsible for diffuse neuro-axonal loss and neurodegeneration [3, 4, 6]. By contrast, effective repair mechanisms can occur within focal lesions but probably also in normal appearing brain tissue (NABT) [7]. However, our understanding of these complex processes is still fragmentary. The difficulty of acquiring histopathological data on MS patients at various stages of the disease makes it challenging to describe the time course of injury and potential repair mechanisms in MS. Consequently, there is an important need for new imaging techniques to improve in-vivo monitoring of lesion formation, progression and repair in MS [8].

Conventional MRI (cMRI) readily depicts focal WM lesions on T2/FLAIR sequences and is able to distinguish between acute and allegedly chronic lesions, primarily on the evidence of blood-brain barrier breakdown, as indicated by contrast enhancement. T2-hyperintensities in cMRI constitute the keystone of McDonald diagnostic criteria [9] and also make an important contribution to the monitoring of WM lesion burden. Unfortunately, cMRI sequences are not

able to efficiently assess cortical lesions or detect diffuse changes in NABT. This shortcoming is particularly apparent in the poor correlation of imaging results with short and long-term clinical outcomes [10]. Quantitative MRI (qMRI) potentially overcomes these limitations by quantifying physical microstructural properties of cerebral tissue in standardized units. Nevertheless, there exist challenging issues in performing longitudinal qMRI protocols. While qMRI in theoretically independent of the scanner used for acquisition as the parametric images rely on physical measurements of brain tissues, in reality the reproducibility is lower than expected, especially for semi-quantitative MT maps [11, 12]. Despite that, longitudinal analysis can still be accurate when identical sequences are used across scanning time points. In addition, qMRI is more sensitive but also more specific to microstructural properties of CNS tissues. Magnetization transfer ratio (MTR) was regularly linked to cerebral macromolecular content detected by a greater percentage loss of magnetization in voxels with a higher myelin content and axons density [13-15]. Post-mortem studies comparing the relative contribution of these two factors indicate that myelin has a stronger and more direct influence on MTR than the axonal density, which is considered as a T1-dependent effect. Tissue water content (inflammation, edema…), another T1-dependent effect, also accounts for MTR variability [14, 16, 17]. However, the MT saturation (MTsat) map offers a measure which, unlike MTR, is minimally affected by longitudinal relaxation and B1 mapping inhomogeneities [18], increasing its sensitivity to myelin content. Moreover, the brain contrast to noise ratio is larger for the MTsat map than for MTR, thus improving brain tissue segmentation in healthy subjects [14, 19]. Regarding the transverse relaxation time T2*, this measure reflects the effective decay of transverse magnetization T2, when considering intra-voxel magnetic field inhomogeneities. In the CNS, paramagnetic iron and diamagnetic myelin generate microscopic field gradients, thus shortening T2* and increasing the R2* (1/T2*) relaxation rate. Orientation

and density of myelin fibers are also a determining factor of R2* values [20-22]. Concerning the longitudinal relaxation rate R1 (1/T1) in the CNS, its three major determinants are tissue myelination and associated axons, iron and extracellular water contents [22-24]. Finally, proton density (PD) mostly reflects the free water content of the brain [25].

We have previously shown that a multivariate qMRI approach is useful to assess NABT microstructural alteration in a cross-sectional study comparing MS patients to healthy controls [26, 27]. Because each qMRI parameter is differently sensitive to histologically measured iron and myelin contents, this approach constitutes a fundamental tool for longitudinal *in-vivo* monitoring of MS lesions and NABT evolution at the tissue microstructural level.

In this longitudinal study, we investigate the evolution of four simultaneously acquired qMRI parameters (MTsat, PD, R1, R2*) within NABT and WM lesions of 17 MS patients (relapsing remitting (RRMS) and progressive MS (PMS)) who were scanned two or three times with at least a one-year interval, following the same multi-parameter mapping (MPM) protocol at 3 Tesla [13, 28]. Segmentation of different cerebral tissue classes was computed using an advanced segmentation technique called Unified Segmentation with Lesion (USwL), an updated version of the traditional Unified Segmentation (US) algorithm from SPM. This pipeline accounts for lesions and relies on quantitative parameter maps rather than the standard weighted images.

Here, we assessed the time course of parameter values in several tissue classes: NAWM, normal appearing cortical and deep GM (NACGM and NADGM) as well as focal WM lesions. In addition, we related the changes in NABT to clinical course.

2. Materials and methods

2.1 Population

Seventeen patients, recruited at the specialized MS outpatient clinic of the CHU Liège, Belgium, with a diagnosis of MS according to the McDonald criteria 2010 [29], were gathered from two studies: ten of them were part of the work reported by Lommers et al. 2019 [26], the other seven were recruited from another MS study taking place at the GIGA Cyclotron Research Centre – In Vivo Imaging (Liège, Belgium). Both were approved by the local ethics committee (approval numbers B707201213806 and B707201835630, respectively). All patients were followed up and scanned twice on the same 3T MRI scanner, every 1 to 3 years. For each of the 17 MS patients, data from two MRI sessions were available, at T0 and T1. This cohort included 11 RRMS patients and 6 (primary and secondary) PMS. Thirteen were receiving disease-modifying treatments (DMTs). The patients' median age was 36 years (range: 25-65) and the median time interval between two scans was 30 months (range: 14-61). Demographic data appears in Table 1. Extended individual information appears in Supplementary data.

	All Patients (n = 17)	
Age, y, median (range)	36 (25-65)	
Sex, F/M	7/10	
MS phenotype (RRMS/MS)	11/6	
Baseline disease duration, y, median (range)	3.4 (0.3-28)	
Baseline EDSS, median (range)	2.5 (1-6.5)	
Baseline number of relapses, median (range)	**RRMS**: 2 (1-5)	**PMS**: N/A
Disease-modifying treatment	**RRMS**: First line, n: 5 Second line, n: 6	**PMS**: Ocrelizumab, n: 2 None, n: 4

Table 1: Demographic data of the study sample

2.2 MR image acquisition

MRI data were acquired on a 3T whole-body MRI-scanner (Magnetom Prisma, Siemens Medical Solutions, Erlangen, Germany). The whole-brain MRI acquisitions included a multi-parameter mapping protocol (MPM), from which one can simultaneously estimate (semi)quantitative maps of magnetization transfer saturation (MTsat), proton density (PD), transverse relaxation (R1) and effective longitudinal relaxation (R2*). This protocol arising from an international collaborative effort [13, 28], has already been used to study brain microstructure in various conditions including normal aging [28, 30, 31], brain tumor [32], Parkinson's disease [33-35] as well as MS. It consists of three co-localized 3D multi-echo fast low angle shot (FLASH) acquisitions at 1mm^3 resolution and two additional calibration sequences to correct for inhomogeneities in the RF transmit field [36, 37]. The FLASH datasets

were acquired with predominantly PD, T1 and MT weighting, referred to in the following as PDw, T1w and MTw echoes. All three had high bandwidth to minimize off-resonance and chemical shift artifacts. Volumes were acquired in 176 sagittal slices using a 256x224 voxel matrix. GRAPPA parallel imaging was combined with partial Fourier acquisition to speed up acquisition time to approximately 20 min. An additional FLAIR sequence was recorded with spatial resolution 1mm^3 and TR/TE/TI=5000ms/516ms/1800ms. Extra B1 field mapping images (transmit B+ and receive B- fields) were also acquired to reduce spatial heterogeneities related to B1 effect. This was essential for proper quantification of T1 (or R1=1/T1) in particular. Finally, B0 field mapping images, corresponding to both magnitude images and pre-subtracted phase image, were acquired for image distortions corrections. A summary of the acquisition parameters appears in Supplementary data.

2.3 MR image processing

All data processing was performed in Matlab (The MathWorks Inc., Natick, MA, USA) using SPM12 (www.fil.ion.ucl.ac.uk/spm) and three additional dedicated SPM extensions: the Lesion Segmentation Tool (LST) version 1.2.3 (www.statisticalmodelling.de/lst.html) [38], the "quantitative MRI and in vivo histology using MRI" toolbox (hMRI, http://hmri.info) [13], and "US-with-Lesion" tool (USwL, https://github.com/CyclotronResearchCentre/USwLesion).

Quantitative maps - MTsat, PD, R1 and R2*- were estimated using the hMRI toolbox. T1w, PDw and MTw images acquired at multiple echo times (TE) were extrapolated to TE=0 to increase signal-to-noise ratio and remove the otherwise remaining R2* bias [13, 26, 39]. The TE=0 extrapolated MTw, PDw and T1w images were used to calculate MT saturation, R1 and apparent signal amplitude A* maps. PD maps were derived from A* maps, which are proportional to proton density. All quantitative maps were corrected for inhomogeneities

from local RF transmit field (B1+), and R1 quantitative maps were further corrected for imperfect RF spoiling using the strategy of Preibisch and Deichmann [40]. The receive bias field map (B1-) was used to correct PD maps for instrumental biases. The R2* map was estimated from all three multi-echo series (MTw, PDw and R1w) using the ESTATICS model [39].

For all sessions, spatial preprocessing involved different steps (Figure 1) after generating quantitative maps using the hMRI toolbox: within-patient registration brought the two serial MR data sets into the individual T0 space, using the longitudinal registration tool from SPM [41]. For each individual patient, a preliminary WM lesion mask was generated based on FLAIR and T1w images by the lesion growth algorithm implemented in the LST toolbox [38], followed by manual corrections by an MS expert (EL) to remove aberrant/artefactual lesion detections [26]. The images were then segmented using the USwL toolbox, which consists of an extended version of the traditional Unified Segmentation (US) algorithm [42] and includes an additional tissue class representing the WM lesion(s). The USwL method internally generates a subject-specific extended set of tissue probability maps (TPM) [43]: an extra tissue class, based on the smoothed preliminary lesion mask warped into template space (using cost function masking during normalization [44]), is added to account for the lesion, and the original white matter prior map is updated accordingly [45]. The grey matter TPM was not updated due to a very low number of lesions present in the cortical ribbon. Multi-channel segmentation was conducted, using MTsat, PD, R1 and FLAIR images. This pipeline did not use the PD-, T1- and MT-weighted images acquired for the MPM maps construction, but the parametric maps themselves instead. In this way, voxels do not depict MR intensities but rather physical quantitative parameters. The method generated the segmented tissue classes (*a posteriori* tissue, including lesion, probability maps), as well as spatial warping into standard template space. The preliminary lesion mask was used as input for the first session data (at T0) then the

228 *a posteriori* lesion map generated at this initial step served as prior to the subsequent session
229 (at T1).
230 Segmentation teased out the different tissue classes of interest: NAWM, NACGM and NADGM,
231 as well as WM lesions. To analyze the microstructure within those tissue classes, *a posteriori*
232 tissue maps were binarized and tissue-specific independent masks were constructed: each
233 voxel is assigned to one single tissue class with the highest probability for that voxel (provided
234 that this probability was above 0.2). The lesion binary mask was further cleaned for lesions
235 <10mm^3 which likely resulted from segmentation errors. Finally, binarized tissue class masks
236 were in turn applied on the MPM maps to extract voxel values inside them.
237

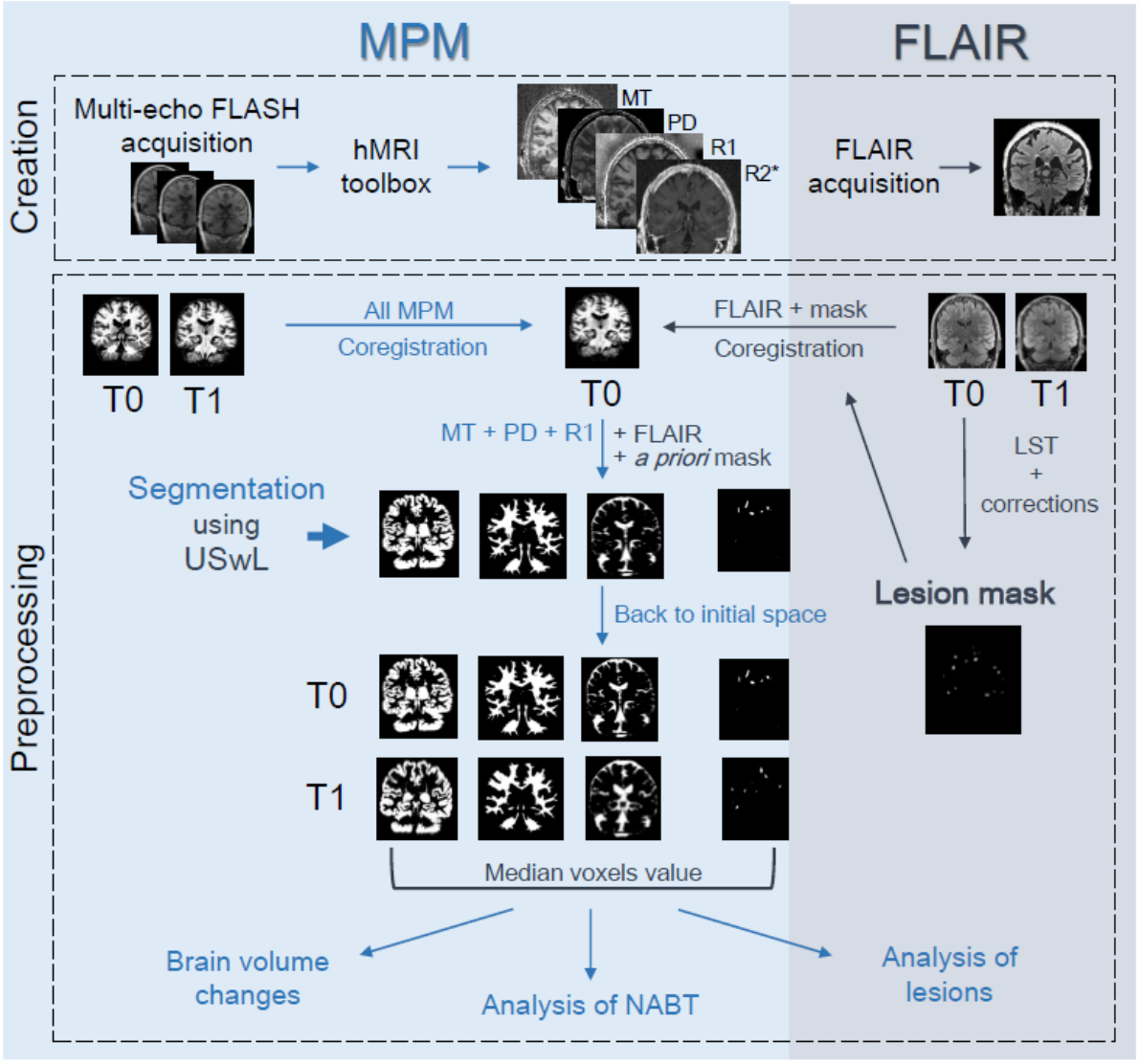

Figure 1: Chartflow of data creation and processing (see text). MPM maps were created with the hMRI-toolbox, FLAIR images were directly acquired for both sessions (T0 and T1). A preliminary mask was constructed based on T0 FLAIR. All images (MPM and FLAIR, T0 and T1) were co-registered to the MPM T0 space. Segmentation using USwL allowed to isolate the different tissue classes.

2.4 Brain volume change

Volumetric changes were investigated using the USwL *a posteriori* tissue probability maps. The following measures of brain volume were computed for each session of each participant: (1) Total intra-cranial volume (TIV)=volume (NAWM + GM + CSF + lesions), (2) brain parenchymal fraction (BPF)=volume (NAWM + GM + lesions)/TIV, (3) GM fraction (GMF)=volume (GM)/TIV, and (4) lesion fraction (LF)=volume (lesion)/TIV. The percentage of change between both scanning sessions was evaluated for each volumetric measurement, then annualized changes were computed by dividing these measures by scan intervals (in years). Results were directly analysed with a t-test (testing if significantly different from 0 at $p < .05$), but also in the same way as the normal-appearing tissues MR parameters in relation to the patients' clinical status (see next section).

2.5 Analysis of normal-appearing tissues

The median value of quantitative MRI parameters was extracted from the three normal-appearing tissues (NAWM, NACGM and NADGM), and an individual annual rate of change (ARoC) was computed for each parameter in each tissue class, based on the initial and final values and accounting for the time interval (in years) between scans. This rate of change in qMRI parameters served as dependent variable in a general linear model testing the effect of clinical status:

$$Y = \beta_0 + \beta_1 X_{status} + \epsilon$$

Y is the ARoC for a qMRI parameter and tissue class, β's are the regression parameters corresponding to the associated regressor (with β_0 the intercept), and ϵ the residuals. X_{status} is a binary categorical variable representing the patient's disease activity status: a status score of 1 was assigned to patients stable or improving from T0 to T1.

This patient status X_{status} was derived from one of two scores of disease activity. For evaluating RRMS patients, NEDA-3 (No Evidence of Disease Activity [46]), a composite of three related measures of disease activity, was used. A score of 0 was assigned in the presence of new clinical relapses and/or MRI activity (new or enlarged lesions visible on FLAIR T2 or Gadolinium-enhanced images) and/or disability progression based on Expanded Disability Status Scale (EDSS). For the PMS patients, disability progression captured by sustained EDSS changes over 6 months (Confirmed Disability Progression [47] at 6 months) indicated disability progression, resulting in a score of 0. For both RRMS and PMS patients, disability progression was defined as a 1.0 point increase if the EDSS score was ≤ 4.0 at baseline and as a 0.5 point increased if the baseline EDSS score was > 4.0. The threshold of 4.0 was proposed in this study because it is considered as a milestone regarding ambulatory performance. NEDA-3 and 6-month CDP were evaluated at mid- and end-scanning interval, and a final status score of 0 was given only to patients for which disease activity or progression was noted in both cases, indicating a clear progression of the disease over the whole interscan interval.

The influence of several clinical measurements such as 25 FWT, 9HPT and SDMT was also considered to refine the evaluation of disease activity. However complete data were lacking for several patients. Moreover, when available, these additional clinical parameters did not modify the final X_{status}.

Permutation tests were employed for inferences [48]. R-squared value was tested against computed statistics after permutation of the data. For a number *n* of permutations, the X_{status} values were randomly shuffled (constructing a new regressor written X_{status}^{π}), tested against the unchanged response Y, and generating each time a permuted R-squared value (noted R_{π}, R_{obs} being the true R-squared value computed without permutation of the data).

The condition $X_{status} \neq X_{status}^{\pi}$ is verified at each permutation. After *n* permutations (with *n = 5000* in this study), a *p*-value was computed based on the following formula:

$$p = \frac{\#(R_\pi > R_{obs})}{n+1}$$

which estimates the probability of obtaining R_{obs} under the null hypothesis that *Y* is not correlated to X_{status}.The null hypothesis is rejected if $p < .05$ FDR-corrected for multiple comparisons [49], for the 12 tests performed (3 tissue classes with 4 qMRI parameters).

Two-tailed t-tests were applied *post-hoc* on the significant results of permutation tests to compare the ARoC distribution between disease status, i.e., $X_{status} = 0$ against $X_{status} = 1$. Inferences were conducted at a significance level of .05.

The same pipeline was applied to the brain volumetric changes (BPF, GMF and LF) to test their correlation to the disease activity status.

2.6 Analysis of lesions and peripheral tissues

For white matter lesions analysis, we did not use ARoC but exploited directly the qMRI parameters voxel values. Importantly, with USwL, the prior lesion mask is only used in a probabilistic way and the estimated posterior lesion map, obtained using MTsat, PD, R1 and FLAIR images, typically showed more extended lesion than clinically visible on the FLAIR image alone, as obtained with LST.

Therefore, we separated focal lesions clinically detected on FLAIR images from their peripheral regions detected on qMRI maps. Two different peripheral regions were considered: one for each time point (T0 and T1). Therefore, at T0, three distinct lesion-related regions were isolated:

- The lesions, as clinically defined, corresponding to hyperintensity on conventional FLAIR MR image acquired at T0 (referred to as ‘focal FLAIR lesion’).

- The peripheral region detected on qMRI maps at T0, not including the FLAIR lesion (referred to as 'initial peripheral lesion').
- The peripheral region detected with the qMRI maps at T1, computed by masking out the T1 lesion mask with the T0 lesion mask (referred to as 'later peripheral lesion'). This region allows us to determine whether its microstructure at T0 forebodes a full-blown plaque, detectable during follow up.

The three areas were compared between each other and with NAWM, in order to characterize them on a microstructural basis (Figure 2). Only enlarging lesions were considered for these comparisons.

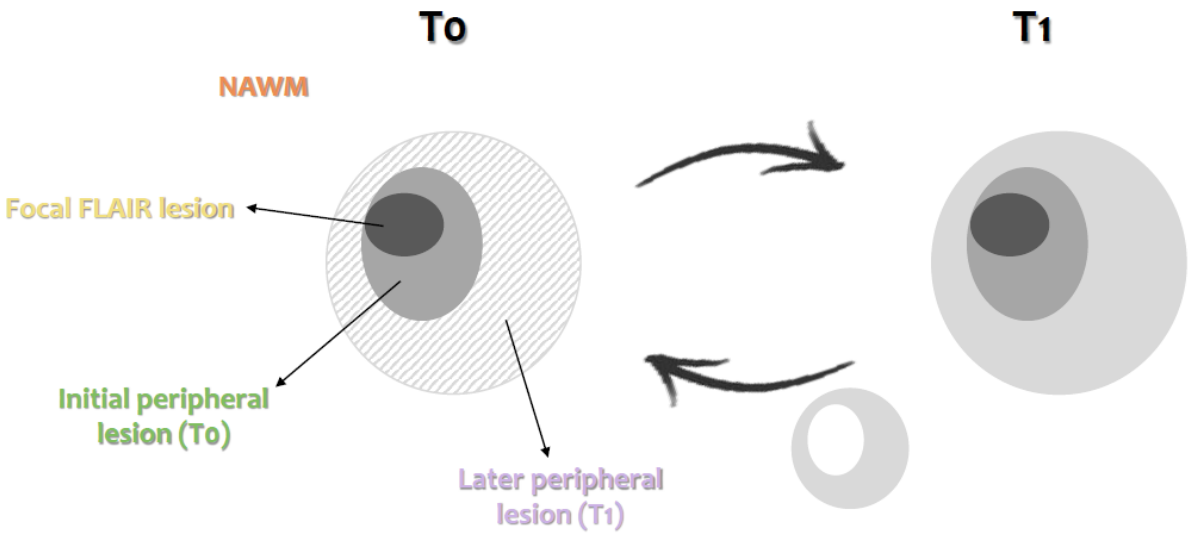

Figure 2: Schematic illustration of the NAWM and 3 lesions-related areas: Focal FLAIR lesion (dark gray area), Initial peripheral lesion detected at T0 (medium gray area), Later peripheral lesion detected at T1 (dashed, left, and light gray, right, area)

NAWM region consisted of all white matter voxels which did not belong to any of the three lesion-related regions. The four areas were independent as no voxel could belong to more than one class at the same time.

For all participants, MTsat, PD, R1 and R2* median values were extracted from each lesion area, considering lesions individually (between 2 and 66 measurements per subject). Similarly, the median qMRI values within NAWM were also extracted (one measurement per subject). These values were extracted from T0 and T1 scans separately. Statistical analyses were performed in SAS 9.4 (SAS Institute, Cary, NC). None of the qMRI parameter was normally distributed, therefore we applied a log transformation on each of them prior to statistical analysis. For each qMRI parameter, a separate Generalized Linear Mixed Model (GLMM) tested the effect of areas (NAWM and the three lesion-related areas), and time points (T0 and T1), as well as their interaction (i.e., area*time), on the median qMRI parameter value, with a first-order autoregressive variance/covariance model and participants as a random factor (intercept). The degrees of freedom were estimated using Kenward-Roger's method. Statistical significance was estimated at $p < .05$ after adjustment for multiple comparison using Tukey's procedure.

3. Results

3.1 Volume changes

BPF annually decreased between T0 and T1 by -0.67 ± 1.12% (significantly different from zero; paired-sample t-tests; $t(16) = 2.57; p = .0204$) whereas LF increased by 22.88 ± 26.13% ($t(16) = -3.70; p = .0019$). GMF non-significantly decreased by -0.30 ± 1.44%.

3.2 Analysis of normal-appearing tissues

As expected, changes in MTsat and R2* within NABT between T0 and T1 varied across subjects (Figure 3). PD and R1 exhibited similar behaviors, see Supplementary data.

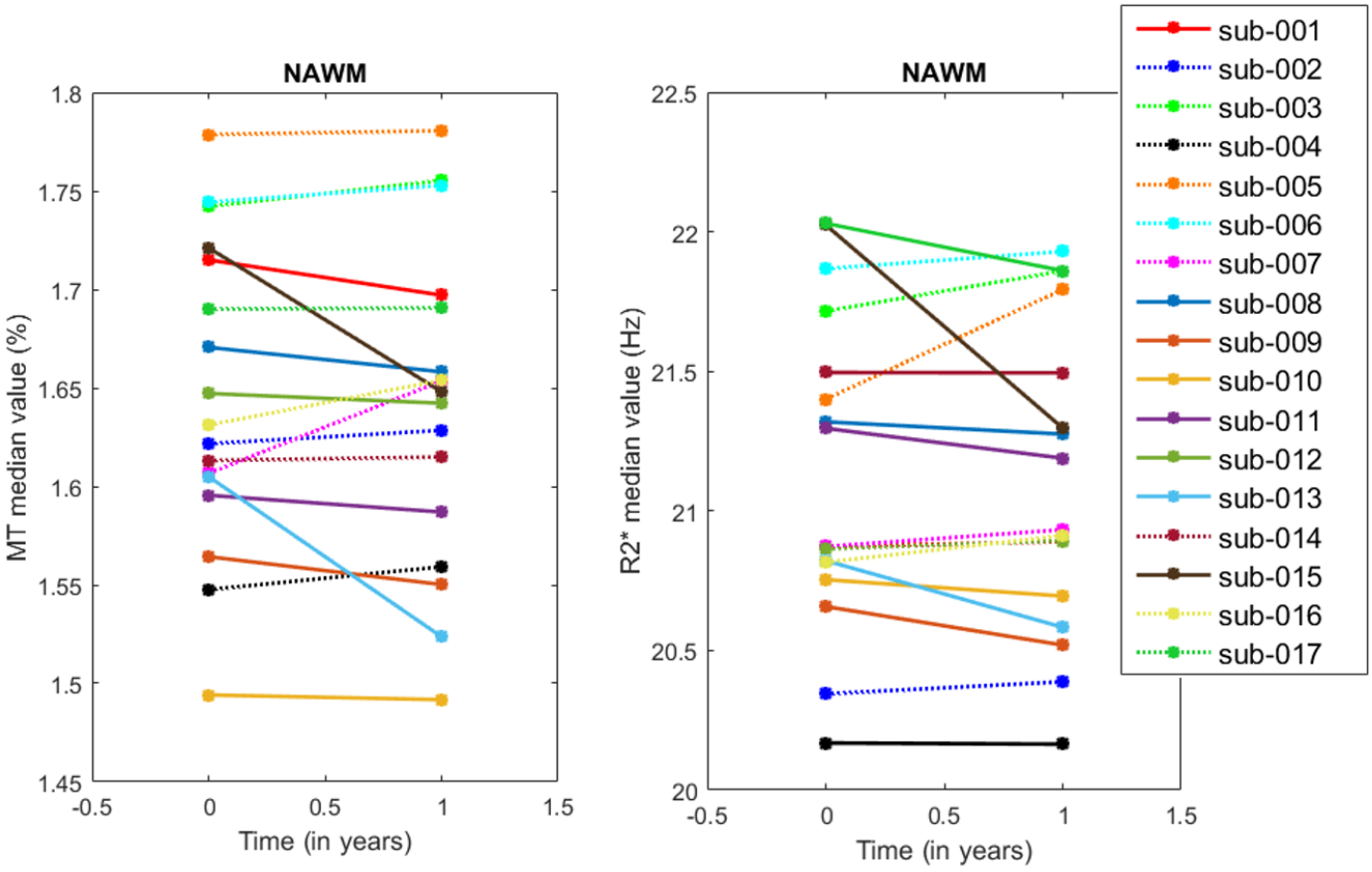

Figure 3: Line plots illustrating individual ARoC's for MTsat (left) and R2* (right) in NAWM. Each line corresponds to one subject. Dotted lines represent increasing rates.

At the group level, with the GLM analysis and permutation inference, we observed that the ARoC of MTsat and R2* positively regressed with disease status as follows (Table 2): MTsat in NAWM and NACGM and R2* in NAWM significantly increase in patients who fare well ($X_{status} = 1$).

	NAWM	NACGM	NADGM
MT	**0.039 (.011)***	**0.017 (.007)***	0.004 (.749)
PD	-0.018 (.670)	0.405 (.225)	0.250 (.552)
R1	0.009 (.139)	0.004 (.471)	0.010 (.111)
R2*	**0.295 (.002)***	0.121 (.092)	0.066 (.770)
BPF	-0.884 (.1562)		
LF	21.23 (.1082)		

Table 2: Regression coefficients and their associated *p*-values (in parentheses) for the effects of X_{status} on the individual ARoC for each qMRI parameter (MTsat, PD, R1 and R2*) and for volumetric measurements (BPF and LF).

* Results significant at $p < .05$, FDR corrected.

Post-hoc t-tests applied on these significant results for a clearer illustration of the difference in disease status (Figure 4) were all significant at a level of .05.

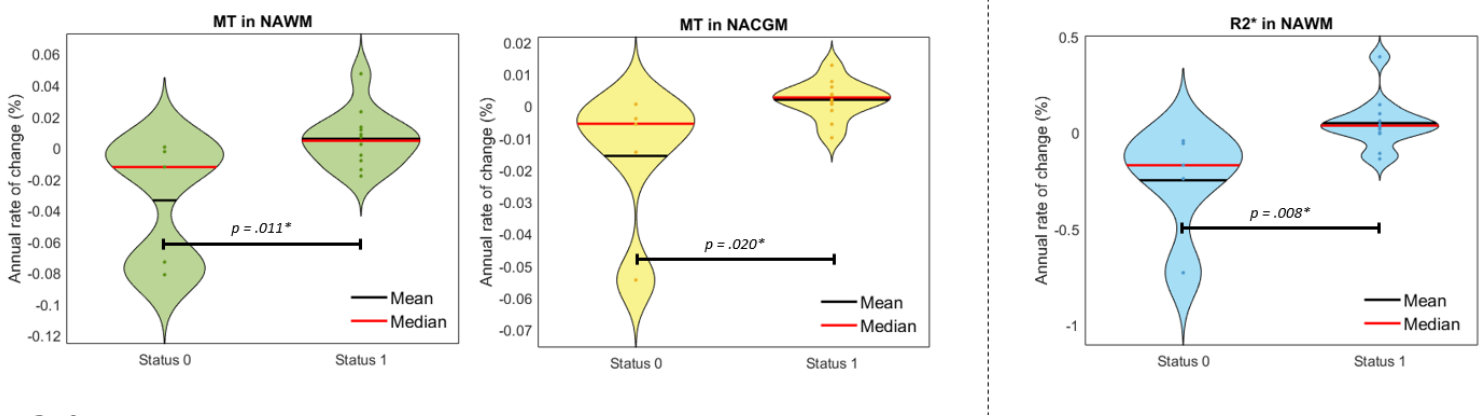

Figure 4: Violin plots of significant change rates in microstructure with respect to X_{status}. From left to right: MT in NAWM, MT in NACGM, R2* in NAWM. * $P < .05$.

Regarding BPF and LF, their correlation to the disease activity status was not significant (Table 2), suggesting that qMRI parameters are more sensitive to subtle microstructural changes in NABT over time than global morphological measurements

3.3 Analysis of lesion microstructure

The number of enlarging WM lesions between T0 and T1 varied from 2 to 66 across patients, corresponding on average to 63% (±31%) of the number of initial focal lesions. The number of enlarging lesions did not significantly differ between patients' disease status groups ($t(15) = .244, p = .811$). GLMMs found a significant effect of areas (3 lesion regions and NAWM) for MT, R1, R2* and PD median (MT: $F_3 = 35.34,\ p < .0001$, PD: $F_3 = 68.03,\ p < .0001$, R1: $F_3 = 40.26,\ p < .0001$, R2*: $F_3 = 32.32,\ p < .0001$). By contrast, neither time effect (T0 vs T1; MT: $F_3 = 0.36,\ p = .5481$, PD: $F_3 = 1.20,\ p = .2735$, R1: $F_3 = 2.05,\ p = .1520$, R2*: $F_3 = 2.86,\ p = .0911$), nor the area*time interaction (MT: $F_3 = 0.09,\ p = .9671$, PD: $F_3 = 0.14,\ p = .9346$, R1: $F_3 = 0.14,\ p = .9331$, R2*: $F_3 = 0.40,\ p = .7565$) were significant, suggesting the microstructural stability of the initial lesion core. *Post-hoc* tests confirmed significant differences between the four tissue areas.

MTsat, R1 and R2* were significantly larger from FLAIR lesion to initial peripheral lesion, from initial to later peripheral lesion and from later peripheral lesion to NAWM. The reverse was observed for PD. The significant difference in parameters between initial and later peripheral lesion at T0 suggests that subtle microstructural changes appear in the periphery of the initial lesion, months before their detection as focal FLAIR lesions at T1. Adjusted *p*-values appear in Figure 5. Detailed statistical results of the GLMM's appear in Supplementary data.

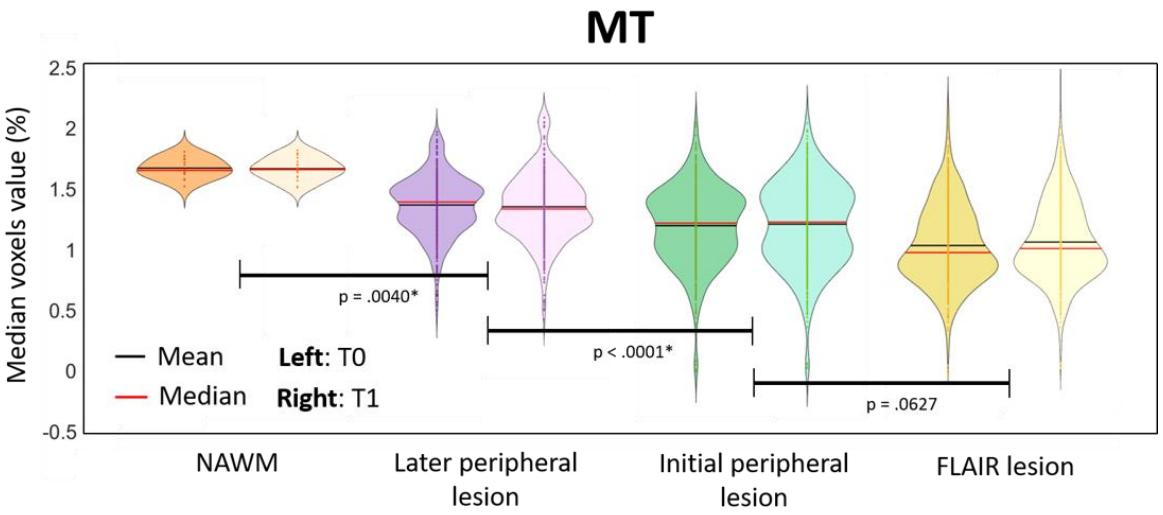

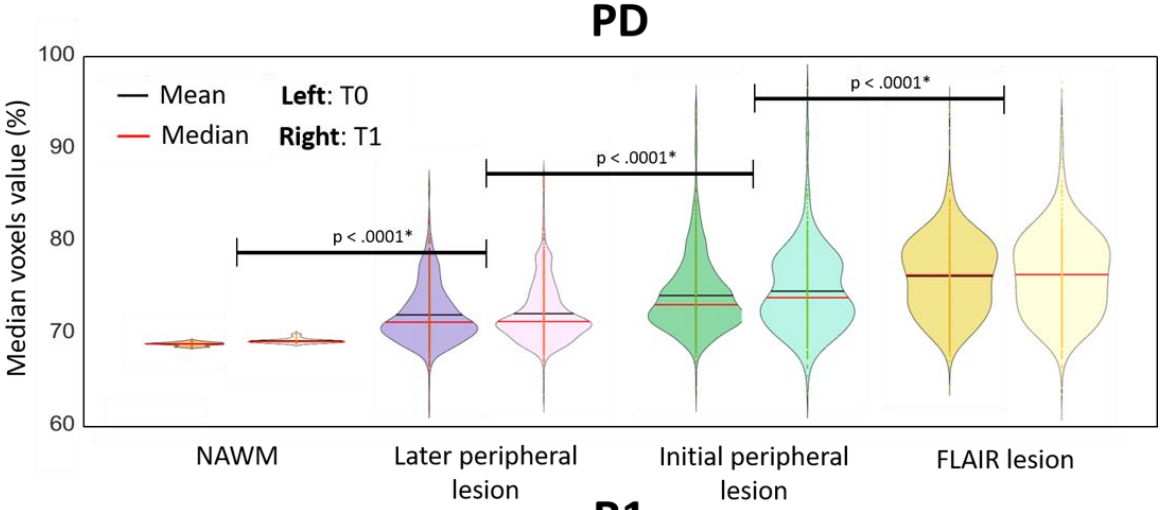

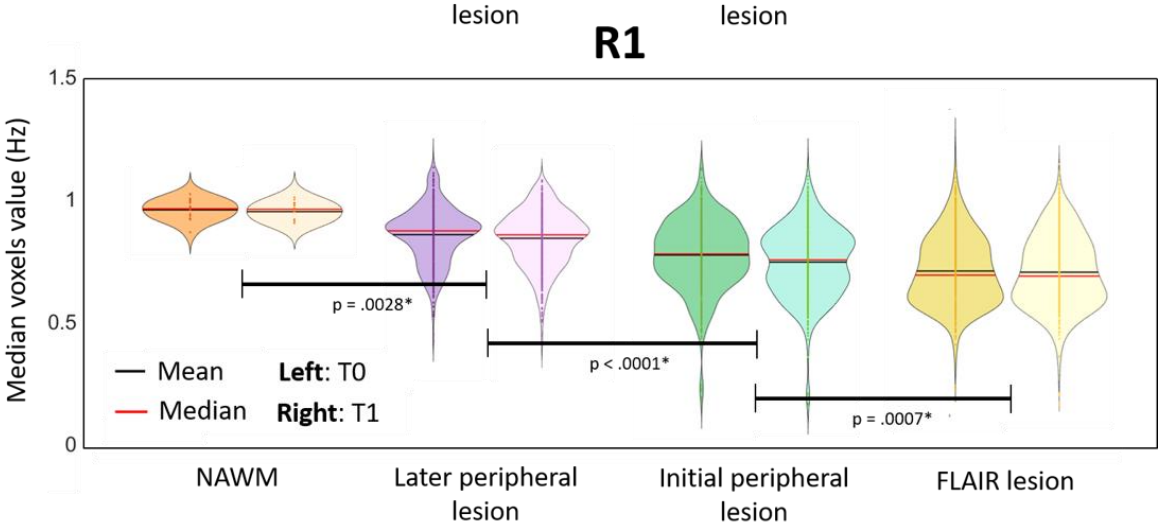

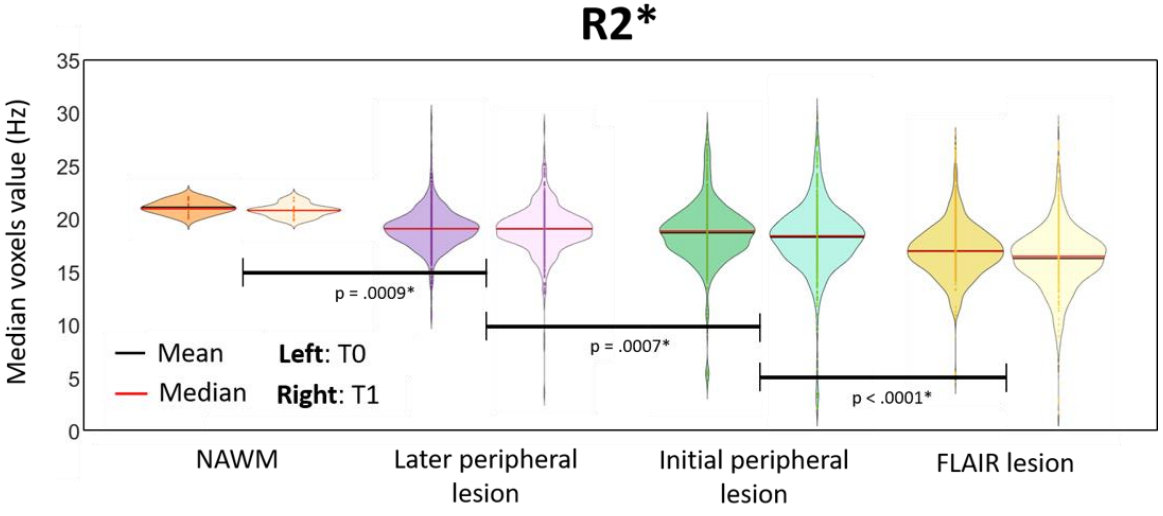

Figure 5: Microstructural parameters in NAWM and the 3 lesion-related areas, for each scanning time T0 and T1. P-values were obtained with *post-hoc* tests on the tissue area effect. * $P < .05$.

4. Discussion

This longitudinal study followed up volumetric data and qMRI brain metrics (MTsat, PD, R1, R2*) in 17 MS patients for a median time interval of 30 months. The main results are threefold. First, the microstructure of normal appearing brain tissues changes over time and these modifications concur with, and potentially drive, clinical evolution. This critical finding suggests that repair mechanism and edema resorption can be monitored *in vivo*. Second, the microstructure within WM plaques is remarkably heterogeneous. Importantly, at their periphery, microstructural alterations foreshadow their expansion, as detected by conventional MRI. Third, as expected, we observed a small but significant brain atrophy and lesion load increase with time.

Quantitative MRI parameter time course within NABT

In this study, we used a multiparameter mapping protocol that was gradually optimized and validated for multi-centric studies [12]. It provides high-resolution maps of multiple qMRI parameters from data acquired during a single scanning session of acceptable duration. A number of cross-sectional studies using a combination of MT, R1, R2* or PD parameters reported significant changes in the microstructure of NABT in MS [26, 50-56]. By contrast, longitudinal analyses of multiparameter qMRI data are scarce. A progressive shortening of T2/T2* [57] or increase in R2* [58-60] was reported within the basal ganglia, suggesting increased of myelin and/or iron contents as well as edema resorption. Likewise, PD and T1 increased within a year, suggesting a demyelination and/or axonal loss [61]. MTR progressively

decreases in NAWM of MS patients over one [62] or two years [63]. These abnormalities tend to be more pronounced in progressive phenotypes [64] and were associated to a slow, diffuse and global myelin pathology.

Here, we showed that MTsat within NAWM and NACGM and R2* values within NAWM increase in clinically stable or improving patients. Because MTsat and R2* both correlate with myelin content [14, 30, 31, 65-67], our results suggest repair mechanisms within NABT of patients who are responding to disease modifying treatments, despite the initial myelin/axonal loss and independently from WM focal lesion evolution. These results echo cross-sectional analyses showing that healthy controls (HC) have higher MTsat and R2* values within the same tissue classes compared to MS patients [26]. Annual rates of change of R1 and PD within NABT were not significantly associated with the individual clinical status in this study, although R1 reduction within NABT has already been reported in cross sectional [26, 53, 54] and longitudinal [61] studies comparing MS subjects to HC.

Lesion microstructure

Focal inflammatory demyelinating lesions have been extensively characterized and are traditionally classified as active, chronic active (smoldering) or inactive plaques according to the presence and distribution of plaque-infiltrating macrophages/microglia [68-70]. Focal WM pathology is a constantly evolving process including episodes of demyelination and remyelination but also accumulation of irreversible axonal damage. Age, disease duration, clinical phenotype as well as disease modifying treatment all contribute to the dynamic nature of focal WM pathology [69, 71]. This accounts for the large inter- and intra-individual heterogeneity of MS, which conventional MRI is largely unable to capture. By contrast, quantitative MRI parameters are sensitive to myelin, axonal as well as iron contents and appear as promising markers of plaque dynamics. For instance, MTR was shown to sharply

452 decrease within gadolinium enhancing lesions before recovering during the subsequent
453 months [72-74]. Likewise, reduction of MTR within NAWM, days to weeks before the
454 formation of a new active lesion was also demonstrated [75, 76], and long-term MTR changes
455 in WM plaques were observed in relation with disease progression [64, 77]. The present study
456 broadens the quantitative characterization of plaque dynamics, in keeping with previous
457 longitudinal studies [57, 78]. Two important findings emerge from the results. First, qMRI
458 refines lesion segmentation, as compared to the processing based on the sole FLAIR image. In
459 consequence, the initial lesion revealed by qMRI is typically wider that the plaque detected in
460 FLAIR. Its periphery is characterized by a decrease in MTsat and R2* as compared to NAWM,
461 suggesting an incipient demyelination, reminiscent of the so-called 'periplaques' [79].
462 Moreover, MTsat, R2* and R1 values progressively decrease from NAWM to plaque core,
463 suggesting a centripetal loss of myelin content. Second, plaque microstructure is altered in
464 plaque periphery before any observable change in conventional MRI signals. This finding
465 suggests, in keeping with neuropathological observations [69, 71, 80, 81] that subclinical
466 ongoing inflammation and/or demyelination takes place in the periphery of an active plaque,
467 well before it is detectable on FLAIR or T1 post-gadolinium sequences. If confirmed on larger
468 population samples, this finding might significantly modify treatment management in MS
469 patients.
470 Oddly enough, plaque qMRI parameters did not significantly change across time. Because iron
471 concentration increases within chronic active or smoldering lesions [82, 83], we were
472 expecting a progressive increase in R2* value. This negative result might be due to the small
473 sample size, the short period of follow up or the limited sensitivity of R2* to local iron
474 concentration as compared to the combined use of R2* and quantitative susceptibility
475 mapping (QSM) [21].

476 **Volumetric Data**

477 CNS atrophy occurs in all stages of MS, since the preclinical phase of the disease and
478 progresses throughout its course, at a much higher rate than one reported in normal aging
479 [84-87]. In this study, the annual brain percentage volume loss at the group level was > 0.4%,
480 which is in line with previous publications [88]. We also showed a significant increase in lesion
481 fraction. Volumetric data (ARoC's) were highly variable across subjects: changes in BPF range
482 from -2.52 to 1.17% and LF from -0.78 to 103.06%. This variability arises from a large number
483 of factors which do or do not relate to MS: age, disease duration, disease phenotype, disease
484 modifying treatment, circadian rhythm, hydration… [86, 87].
485 Moreover, annual changes in brain parenchymal fraction as well as lesion fraction only
486 partially correlated to patients' disease status, in accordance with a large amount of
487 publications [61, 89]. This highlights the lack of specificity and sensitivity of volumetric
488 measurements, at least at the individual level.

489 **Study limitation**

490 As mentioned earlier, the main limitation of the study was the small size and heterogeneous
491 aspect of the present dataset. Indeed, it is composed of only 17 patients, with a rather broad
492 range of characteristics such as age, disease duration, disease phenotype, disease modifying
493 treatment, etc., which are known to influence the disability state of the patient and thus their
494 ability to put together repair mechanisms within cerebral tissues [1, 69-71, 90, 91]. In addition,
495 the time interval between two scanning sessions varied quite a lot across patients (between
496 14 and 61 months), although it was brought back to an annual rate where possible. All of these
497 features were imposed by standard clinical follow up. Therefore, these results should not be
498 over-interpreted but are nevertheless promising and call for a replication with a larger and
499 more homogeneous or controlled set of MS patients.

5. Conclusion

These preliminary results highlight the relevance of multiple qMRI data in the monitoring of subtle changes within NABT and plaque dynamics in relation with repair or disease progression. Of course, large scale longitudinal study would be needed to reproduce these findings and better exploit the full potential of qMRI parameters.

6. Declarations of interest

None.

7. Funding

NV, EL and CP are supported by the Fonds de la Recherche Scientifique (F.R.S-FNRS Belgium)

8. References

[1] Lassmann, Hans. "Pathology and Disease Mechanisms in Different Stages of Multiple Sclerosis." *Journal of the Neurological Sciences* 333, no. 1–2 (October 2013): 1–4. https://doi.org/10.1016/j.jns.2013.05.010.

[2] Trapp, Bruce D., John Peterson, Richard M. Ransohoff, Richard Rudick, Sverre Mörk, and Lars Bö. "Axonal Transection in the Lesions of Multiple Sclerosis." *New England Journal of Medicine* 338, no. 5 (January 29, 1998): 278–85. https://doi.org/10.1056/NEJM199801293380502.

[3] Haider, Lukas, Tobias Zrzavy, Simon Hametner, Romana Höftberger, Francesca Bagnato, Günther Grabner, Siegfried Trattnig, Sabine Pfeifenbring, Wolfgang Brück, and Hans Lassmann. "The Topograpy of Demyelination and Neurodegeneration in the Multiple Sclerosis Brain." *Brain* 139, no. 3 (March 2016): 807–15. https://doi.org/10.1093/brain/awv398.

[4] Kutzelnigg, Alexandra, Claudia F. Lucchinetti, Christine Stadelmann, Wolfgang Brück, Helmut Rauschka, Markus Bergmann, Manfred Schmidbauer, Joseph E. Parisi, and Hans Lassmann. "Cortical Demyelination and Diffuse White Matter Injury in Multiple Sclerosis." *Brain* 128, no. 11 (November 1, 2005): 2705–12. https://doi.org/10.1093/brain/awh641.

[5] Gh Popescu, Bogdan F, and Claudia F Lucchinetti. "Meningeal and Cortical Grey Matter Pathology in Multiple Sclerosis." *BMC Neurology* 12, no. 1 (December 2012): 11. https://doi.org/10.1186/1471-2377-12-11.

[6] Frischer, Josa M., Stephan Bramow, Assunta Dal-Bianco, Claudia F. Lucchinetti, Helmut Rauschka, Manfred Schmidbauer, Henning Laursen, Per Soelberg Sorensen, and Hans Lassmann. "The Relation between Inflammation and Neurodegeneration in Multiple Sclerosis Brains." *Brain* 132, no. 5 (May 2009): 1175–89. https://doi.org/10.1093/brain/awp070.

[7] Brown, Robert A., Sridar Narayanan, and Douglas L. Arnold. "Imaging of Repeated Episodes of Demyelination and Remyelination in Multiple Sclerosis." *NeuroImage: Clinical* 6 (2014): 20–25. https://doi.org/10.1016/j.nicl.2014.06.009.

[8] Wang, Chenyu Tim, Michael Barnett, and Yael Barnett. "Imaging the Multiple Sclerosis Lesion: Insights into Pathogenesis, Progression and Repair." *Current Opinion in Neurology* 32, no. 3 (June 2019): 338–45. https://doi.org/10.1097/WCO.0000000000000698.

[9] Thompson, Alan J, Brenda L Banwell, Frederik Barkhof, William M Carroll, Timothy Coetzee, Giancarlo Comi, Jorge Correale, et al. "Diagnosis of Multiple Sclerosis: 2017 Revisions of the McDonald Criteria." *The Lancet Neurology* 17, no. 2 (February 2018): 162–73. https://doi.org/10.1016/S1474-4422(17)30470-2.

561 [10] Barkhof, Frederik. "The Clinico-Radiological Paradox in Multiple Sclerosis
562 Revisited:" *Current Opinion in Neurology* 15, no. 3 (June 2002): 239–45.
563 https://doi.org/10.1097/00019052-200206000-00003.
564
565 [11] Gracien, René-Maxime, Michelle Maiworm, Nadine Brüche, Manoj Shrestha,
566 Ulrike Nöth, Elke Hattingen, Marlies Wagner, and Ralf Deichmann. "How Stable Is
567 Quantitative MRI? – Assessment of Intra- and Inter-Scanner-Model Reproducibility
568 Using Identical Acquisition Sequences and Data Analysis Programs." *NeuroImage* 207
569 (February 2020): 116364. https://doi.org/10.1016/j.neuroimage.2019.116364.
570
571 [12] Leutritz, Tobias, Maryam Seif, Gunther Helms, Rebecca S Samson, Armin Curt,
572 Patrick Freund, and Nikolaus Weiskopf. "Multiparameter Mapping of Relaxation (R1 ,
573 R2 *), Proton Density and Magnetization Transfer Saturation at 3 T : A Multicenter Dual-
574 vendor Reproducibility and Repeatability Study." *Human Brain Mapping* 41, no. 15
575 (October 15, 2020): 4232–47. https://doi.org/10.1002/hbm.25122.
576
577 [13] Tabelow, Karsten, Evelyne Balteau, John Ashburner, Martina F. Callaghan, Bogdan
578 Draganski, Gunther Helms, Ferath Kherif, et al. "HMRI – A Toolbox for Quantitative MRI
579 in Neuroscience and Clinical Research." *NeuroImage* 194 (July 2019): 191–210.
580 https://doi.org/10.1016/j.neuroimage.2019.01.029.
581
582 [14] Schmierer, Klaus, Francesco Scaravilli, Daniel R. Altmann, Gareth J. Barker, and
583 David H. Miller. "Magnetization Transfer Ratio and Myelin in Postmortem Multiple

584 Sclerosis Brain." *Annals of Neurology* 56, no. 3 (September 2004): 407–15.
585 https://doi.org/10.1002/ana.20202.
586
587 [15] Callaghan, Martina F., Gunther Helms, Antoine Lutti, Siawoosh Mohammadi, and
588 Nikolaus Weiskopf. "A General Linear Relaxometry Model of R $_1$ Using Imaging Data:
589 General Linear Relaxometry Model of R1." *Magnetic Resonance in Medicine* 73, no. 3
590 (March 2015): 1309–14. https://doi.org/10.1002/mrm.25210.
591
592 [16] Van Waesberghe, J. H. T. M., W. Kamphorst, C. J. A. De Groot, M. A. A. Van
593 Walderveen, J. A. Castelijns, R. Ravid, G. J. Lycklama a Nijeholt, et al. "Axonal Loss in
594 Multiple Sclerosis Lesions: Magnetic Resonance Imaging Insights into Substrates of
595 Disability." *Annals of Neurology* 46, no. 5 (November 1999): 747–54.
596 https://doi.org/10.1002/1531-8249(199911)46:5<747::AID-ANA10>3.0.CO;2-4.
597
598 [17] Mottershead, J. P., K. Schmierer, M. Clemence, J. S. Thornton, F. Scaravilli, G. J.
599 Barker, P. S. Tofts, et al. "High Field MRI Correlates of Myelin Content and Axonal
600 Density in Multiple Sclerosis." *Journal of Neurology* 250, no. 11 (November 1, 2003):
601 1293–1301. https://doi.org/10.1007/s00415-003-0192-3.
602
603 [18] Lema, Alfonso, Courtney Bishop, Omar Malik, Miriam Mattoscio, Rehiana Ali,
604 Richard Nicholas, Paolo A. Muraro, Paul M. Matthews, Adam D. Waldman, and Rexford
605 D. Newbould. "A Comparison of Magnetization Transfer Methods to Assess Brain and
606 Cervical Cord Microstructure in Multiple Sclerosis: MT of Brain and c-Spine in MS."

Journal of Neuroimaging 27, no. 2 (March 2017): 221–26. https://doi.org/10.1111/jon.12377.

[19] Helms, Gunther, Henning Dathe, and Peter Dechent. "Modeling the Influence of TR and Excitation Flip Angle on the Magnetization Transfer Ratio (MTR) in Human Brain Obtained from 3D Spoiled Gradient Echo MRI." *Magnetic Resonance in Medicine* 64, no. 1 (July 2010): 177–85. https://doi.org/10.1002/mrm.22379.

[20] Bagnato, Francesca, Simon Hametner, Emma Boyd, Verena Endmayr, Yaping Shi, Vasiliki Ikonomidou, Guanhua Chen, et al. "Untangling the R2* Contrast in Multiple Sclerosis: A Combined MRI-Histology Study at 7.0 Tesla." Edited by Quan Jiang. *PLOS ONE* 13, no. 3 (March 21, 2018): e0193839. https://doi.org/10.1371/journal.pone.0193839.

[21] Hametner, Simon, Verena Endmayr, Andreas Deistung, Pilar Palmrich, Max Prihoda, Evelin Haimburger, Christian Menard, et al. "The Influence of Brain Iron and Myelin on Magnetic Susceptibility and Effective Transverse Relaxation - A Biochemical and Histological Validation Study." *NeuroImage* 179 (October 2018): 117–33. https://doi.org/10.1016/j.neuroimage.2018.06.007.

[22] Stüber, Carsten, Markus Morawski, Andreas Schäfer, Christian Labadie, Miriam Wähnert, Christoph Leuze, Markus Streicher, et al. "Myelin and Iron Concentration in the Human Brain: A Quantitative Study of MRI Contrast." *NeuroImage* 93 (June 2014): 95–106. https://doi.org/10.1016/j.neuroimage.2014.02.026.

[23] Granziera, Cristina, Jens Wuerfel, Frederik Barkhof, Massimiliano Calabrese, Nicola De Stefano, Christian Enzinger, Nikos Evangelou, et al. "Quantitative Magnetic Resonance Imaging towards Clinical Application in Multiple Sclerosis." *Brain* 144, no. 5 (June 22, 2021): 1296–1311. https://doi.org/10.1093/brain/awab029.

[24] Kolb, Hadar, Martina Absinta, Erin S. Beck, Seung-Kwon Ha, Yeajin Song, Gina Norato, Irene Cortese, Pascal Sati, Govind Nair, and Daniel S. Reich. "7T MRI Differentiates Remyelinated from Demyelinated Multiple Sclerosis Lesions." *Annals of Neurology* 90, no. 4 (October 2021): 612–26. https://doi.org/10.1002/ana.26194.

[25] Edwards, Luke J., Evgeniya Kirilina, Siawoosh Mohammadi, and Nikolaus Weiskopf. "Microstructural Imaging of Human Neocortex in Vivo." *NeuroImage* 182 (November 2018): 184–206. https://doi.org/10.1016/j.neuroimage.2018.02.055.

[26] Lommers, Emilie, Jessica Simon, Gilles Reuter, Gaël Delrue, Dominique Dive, Christian Degueldre, Evelyne Balteau, Christophe Phillips, and Pierre Maquet. "Multiparameter MRI Quantification of Microstructural Tissue Alterations in Multiple Sclerosis." *NeuroImage: Clinical* 23 (2019): 101879. https://doi.org/10.1016/j.nicl.2019.101879.

[27] Lommers, Emilie, Camille Guillemin, Gilles Reuter, Eve Fouarge, Gaël Delrue, Fabienne Collette, Christian Degueldre, Evelyne Balteau, Pierre Maquet, and Christophe Phillips. "VOXEL-BASED Quantitative MRI Reveals Spatial Patterns of Grey

655 Matter Alteration in Multiple Sclerosis." *Human Brain Mapping* 42, no. 4 (March 2021):
656 1003–12. https://doi.org/10.1002/hbm.25274.
657
658 [28] Draganski, B., J. Ashburner, C. Hutton, F. Kherif, R.S.J. Frackowiak, G. Helms, and N.
659 Weiskopf. "Regional Specificity of MRI Contrast Parameter Changes in Normal Ageing
660 Revealed by Voxel-Based Quantification (VBQ)." *NeuroImage* 55, no. 4 (April 2011):
661 1423–34. https://doi.org/10.1016/j.neuroimage.2011.01.052.
662
663 [29] Polman, Chris H., Stephen C. Reingold, Brenda Banwell, Michel Clanet, Jeffrey A.
664 Cohen, Massimo Filippi, Kazuo Fujihara, et al. "Diagnostic Criteria for Multiple Sclerosis:
665 2010 Revisions to the McDonald Criteria." *Annals of Neurology* 69, no. 2 (February
666 2011): 292–302. https://doi.org/10.1002/ana.22366.
667
668 [30] Callaghan, Martina F., Patrick Freund, Bogdan Draganski, Elaine Anderson,
669 Marinella Cappelletti, Rumana Chowdhury, Joern Diedrichsen, et al. "Widespread Age-
670 Related Differences in the Human Brain Microstructure Revealed by Quantitative
671 Magnetic Resonance Imaging." *Neurobiology of Aging* 35, no. 8 (August 2014): 1862–
672 72. https://doi.org/10.1016/j.neurobiolaging.2014.02.008.
673
674 [31] Carey, Daniel, Francesco Caprini, Micah Allen, Antoine Lutti, Nikolaus Weiskopf,
675 Geraint Rees, Martina F. Callaghan, and Frederic Dick. "Quantitative MRI Provides
676 Markers of Intra-, Inter-Regional, and Age-Related Differences in Young Adult Cortical
677 Microstructure." *NeuroImage* 182 (November 2018): 429–40.
678 https://doi.org/10.1016/j.neuroimage.2017.11.066.

[32] Reuter, Gilles, Emilie Lommers, Evelyne Balteau, Jessica Simon, Christophe Phillips, Felix Scholtes, Didier Martin, Arnaud Lombard, and Pierre Maquet. "Multiparameter Quantitative Histological MRI Values in High-Grade Gliomas: A Potential Biomarker of Tumor Progression." *Neuro-Oncology Practice* 7, no. 6 (December 4, 2020): 646–55. https://doi.org/10.1093/nop/npaa047.

[33] Depierreux, Frédérique, Eric Parmentier, Laurane Mackels, Katherine Baquero, Christian Degueldre, Evelyne Balteau, Eric Salmon, et al. "Parkinson's Disease Multimodal Imaging: F-DOPA PET, Neuromelanin-Sensitive and Quantitative Iron-Sensitive MRI." *Npj Parkinson's Disease* 7, no. 1 (December 2021): 57. https://doi.org/10.1038/s41531-021-00199-2.

[34] Nürnberger, Lucas, René-Maxime Gracien, Pavel Hok, Stephanie-Michelle Hof, Udo Rüb, Helmuth Steinmetz, Rüdiger Hilker, Johannes C. Klein, Ralf Deichmann, and Simon Baudrexel. "Longitudinal Changes of Cortical Microstructure in Parkinson's Disease Assessed with T1 Relaxometry." *NeuroImage: Clinical* 13 (2017): 405–14. https://doi.org/10.1016/j.nicl.2016.12.025.

[35] Klein, J.C., M. Rolinski, L. Griffanti, K. Szewczyk-Krolikowski, F. Baig, C. Ruffmann, A.R. Groves, R.A.L. Menke, M.T. Hu, and C. Mackay. "Cortical Structural Involvement and Cognitive Dysfunction in Early Parkinson's Disease." *NMR in Biomedicine* 31, no. 4 (April 2018): e3900. https://doi.org/10.1002/nbm.3900.

703 [36] Lutti, Antoine, Chloe Hutton, Jürgen Finsterbusch, Gunther Helms, and Nikolaus
704 Weiskopf. "Optimization and Validation of Methods for Mapping of the Radiofrequency
705 Transmit Field at 3T: Optimized RF Transmit Field Mapping at 3T." *Magnetic Resonance*
706 *in Medicine* 64, no. 1 (July 2010): 229–38. https://doi.org/10.1002/mrm.22421.
707
708 [37] Lutti, Antoine, Joerg Stadler, Oliver Josephs, Christian Windischberger, Oliver
709 Speck, Johannes Bernarding, Chloe Hutton, and Nikolaus Weiskopf. "Robust and Fast
710 Whole Brain Mapping of the RF Transmit Field B1 at 7T." Edited by Wang Zhan. *PLoS*
711 *ONE* 7, no. 3 (March 12, 2012): e32379.
712 https://doi.org/10.1371/journal.pone.0032379.
713
714 [38] Schmidt, Paul, Christian Gaser, Milan Arsic, Dorothea Buck, Annette Förschler,
715 Achim Berthele, Muna Hoshi, et al. "An Automated Tool for Detection of FLAIR-
716 Hyperintense White-Matter Lesions in Multiple Sclerosis." *NeuroImage* 59, no. 4
717 (February 2012): 3774–83. https://doi.org/10.1016/j.neuroimage.2011.11.032.
718
719 [39] Weiskopf, Nikolaus, Martina F. Callaghan, Oliver Josephs, Antoine Lutti, and
720 Siawoosh Mohammadi. "Estimating the Apparent Transverse Relaxation Time (R2*)
721 from Images with Different Contrasts (ESTATICS) Reduces Motion Artifacts." *Frontiers*
722 *in Neuroscience* 8 (September 10, 2014). https://doi.org/10.3389/fnins.2014.00278.
723
724 [40] Preibisch, C., and R. Deichmann. "Influence of RF Spoiling on the Stability and
725 Accuracy of T_1 Mapping Based on Spoiled FLASH with Varying Flip Angles: Influence of

726 RF Spoiling on T_1 Mapping." *Magnetic Resonance in Medicine* 61, no. 1 (January 2009):
727 125–35. https://doi.org/10.1002/mrm.21776.
728
729 [41] Ashburner, John. "Symmetric Diffeomorphic Modeling of Longitudinal Structural
730 MRI." *Frontiers in Neuroscience* 6 (2013). https://doi.org/10.3389/fnins.2012.00197.
731
732 [42] Ashburner, John, and Karl J. Friston. "Unified Segmentation." *NeuroImage* 26, no.
733 3 (July 2005): 839–51. https://doi.org/10.1016/j.neuroimage.2005.02.018.
734
735 [43] Lorio, S., S. Fresard, S. Adaszewski, F. Kherif, R. Chowdhury, R.S. Frackowiak, J.
736 Ashburner, et al. "New Tissue Priors for Improved Automated Classification of
737 Subcortical Brain Structures on MRI." *NeuroImage* 130 (April 2016): 157–66.
738 https://doi.org/10.1016/j.neuroimage.2016.01.062.
739
740 [44] Andersen, Sarah M., Steven Z. Rapcsak, and Pélagie M. Beeson. "Cost Function
741 Masking during Normalization of Brains with Focal Lesions: Still a Necessity?"
742 *NeuroImage* 53, no. 1 (October 2010): 78–84.
743 https://doi.org/10.1016/j.neuroimage.2010.06.003.
744
745 [45] Moon, Nathan, Elizabeth Bullitt, Koen van Leemput, and Guido Gerig. "Automatic
746 Brain and Tumor Segmentation." In *Medical Image Computing and Computer-Assisted*
747 *Intervention — MICCAI 2002*, edited by Takeyoshi Dohi and Ron Kikinis, 2488:372–79.
748 Lecture Notes in Computer Science. Berlin, Heidelberg: Springer Berlin Heidelberg,
749 2002. https://doi.org/10.1007/3-540-45786-0_46.

[46] Pandit, Lekha. "No Evidence of Disease Activity (NEDA) in Multiple Sclerosis - Shifting the Goal Posts." *Annals of Indian Academy of Neurology* 22, no. 3 (2019): 261. https://doi.org/10.4103/aian.AIAN_159_19.

[47] Wiendl, Heinz, and Sven G. Meuth. "Pharmacological Approaches to Delaying Disability Progression in Patients with Multiple Sclerosis." *Drugs* 75, no. 9 (June 2015): 947–77. https://doi.org/10.1007/s40265-015-0411-0.

[48] Anderson, Marti J. "Permutation Tests for Univariate or Multivariate Analysis of Variance and Regression." *Canadian Journal of Fisheries and Aquatic Sciences* 58, no. 3 (March 1, 2001): 626–39. https://doi.org/10.1139/f01-004.

[49] Yoav Benjamini and Yosef Hochberg. "Controlling the False Discovery Rate: a Practical and Powerful Approach to Multiple Testing" *Journal of the Royal Statistical Society. Series B (Methodological)*, Vol. 57, No.1 (1995), 289-300.

[50] Andica, Christina, Akifumi Hagiwara, Koji Kamagata, Kazumasa Yokoyama, Keigo Shimoji, Asami Saito, Yuki Takenaka, et al. "Gray Matter Alterations in Early and Late Relapsing-Remitting Multiple Sclerosis Evaluated with Synthetic Quantitative Magnetic Resonance Imaging." *Scientific Reports* 9, no. 1 (December 2019): 8147. https://doi.org/10.1038/s41598-019-44615-3.

[51] Bonnier, Guillaume, Alexis Roche, David Romascano, Samanta Simioni, Djalel Meskaldji, David Rotzinger, Ying-Chia Lin, et al. "Advanced MRI Unravels the Nature of Tissue Alterations in Early Multiple Sclerosis." *Annals of Clinical and Translational Neurology* 1, no. 6 (June 2014): 423–32. https://doi.org/10.1002/acn3.68.

[52] Engström, Maria, Jan B. M. Warntjes, Anders Tisell, Anne-Marie Landtblom, and Peter Lundberg. "Multi-Parametric Representation of Voxel-Based Quantitative Magnetic Resonance Imaging." Edited by Friedemann Paul. *PLoS ONE* 9, no. 11 (November 13, 2014): e111688. https://doi.org/10.1371/journal.pone.0111688.

[53] Gracien, René-Maxime, Alina Jurcoane, Marlies Wagner, Sarah C. Reitz, Christoph Mayer, Steffen Volz, Stephanie-Michelle Hof, et al. "Multimodal Quantitative MRI Assessment of Cortical Damage in Relapsing-Remitting Multiple Sclerosis: Cortical Quantitative MRI in RRMS." *Journal of Magnetic Resonance Imaging* 44, no. 6 (December 2016): 1600–1607. https://doi.org/10.1002/jmri.25297.

[54] Neema, Mohit, James Stankiewicz, Ashish Arora, Venkata S.R. Dandamudi, Courtney E. Batt, Zachary D. Guss, Ali Al-Sabbagh, and Rohit Bakshi. "T1- and T2-Based MRI Measures of Diffuse Gray Matter and White Matter Damage in Patients with Multiple Sclerosis." *Journal of Neuroimaging* 17 (April 2007): 16S-21S. https://doi.org/10.1111/j.1552-6569.2007.00131.x.

[55] Reitz, Sarah C., Stephanie-Michelle Hof, Vinzenz Fleischer, Alla Brodski, Adriane Gröger, René-Maxime Gracien, Amgad Droby, et al. "Multi-Parametric Quantitative MRI of Normal Appearing White Matter in Multiple Sclerosis, and the Effect of Disease Activity on T2." *Brain Imaging and Behavior* 11, no. 3 (June 2017): 744–53. https://doi.org/10.1007/s11682-016-9550-5.

[56] Stevenson, V.L, G.J.M Parker, G.J Barker, K Birnie, P.S Tofts, D.H Miller, and A.J Thompson. "Variations in T1 and T2 Relaxation Times of Normal Appearing White Matter and Lesions in Multiple Sclerosis." *Journal of the Neurological Sciences* 178, no. 2 (September 2000): 81–87. https://doi.org/10.1016/S0022-510X(00)00339-7.

[57] Bonnier, Guillaume, Benedicte Maréchal, Mário João Fartaria, Pavel Falkowskiy, José P. Marques, Samanta Simioni, Myriam Schluep, et al. "The Combined Quantification and Interpretation of Multiple Quantitative Magnetic Resonance Imaging Metrics Enlightens Longitudinal Changes Compatible with Brain Repair in Relapsing-Remitting Multiple Sclerosis Patients." *Frontiers in Neurology* 8 (September 27, 2017): 506. https://doi.org/10.3389/fneur.2017.00506.

[58] Elkady, Ahmed M., Dana Cobzas, Hongfu Sun, Gregg Blevins, and Alan H. Wilman. "Discriminative Analysis of Regional Evolution of Iron and Myelin/Calcium in Deep Gray Matter of Multiple Sclerosis and Healthy Subjects: Analysis of Iron and Myelin in MS." *Journal of Magnetic Resonance Imaging* 48, no. 3 (September 2018): 652–68. https://doi.org/10.1002/jmri.26004.

[59] Elkady, Ahmed M., Dana Cobzas, Hongfu Sun, Peter Seres, Gregg Blevins, and Alan H. Wilman. "Five Year Iron Changes in Relapsing-Remitting Multiple Sclerosis Deep Gray Matter Compared to Healthy Controls." *Multiple Sclerosis and Related Disorders* 33 (August 2019): 107–15. https://doi.org/10.1016/j.msard.2019.05.028.

[60] Khalil, M., C. Langkammer, A. Pichler, D. Pinter, T. Gattringer, G. Bachmaier, S. Ropele, S. Fuchs, C. Enzinger, and F. Fazekas. "Dynamics of Brain Iron Levels in Multiple Sclerosis: A Longitudinal 3T MRI Study." *Neurology* 84, no. 24 (June 16, 2015): 2396–2402. https://doi.org/10.1212/WNL.0000000000001679.

[61] Gracien, René-Maxime, Sarah C. Reitz, Stephanie-Michelle Hof, Vinzenz Fleischer, Amgad Droby, Mathias Wahl, Helmuth Steinmetz, Sergiu Groppa, Ralf Deichmann, and Johannes C. Klein. "Longitudinal Quantitative MRI Assessment of Cortical Damage in Multiple Sclerosis: A Pilot Study: Longitudinal Cortical QMRI in MS." *Journal of Magnetic Resonance Imaging* 46, no. 5 (November 2017): 1485–90. https://doi.org/10.1002/jmri.25685.

[62] Laule, Cornelia, I. M. Vavasour, K. P. Whittall, J. Oger, D. W. Paty, D. K. B. Li, A. L. MacKay, and D. L. Arnold. "Evolution of Focal and Diffuse magnetisation Transfer Abnormalities in Multiple Sclerosis." *Journal of Neurology* 250, no. 8 (August 2003): 924–31. https://doi.org/10.1007/s00415-003-1115-z.

[63] Hayton, T., J. Furby, K. J. Smith, D. R. Altmann, R. Brenner, J. Chataway, K. Hunter, D. J. Tozer, D. H. Miller, and R. Kapoor. "Longitudinal Changes in Magnetisation Transfer

Ratio in Secondary Progressive Multiple Sclerosis: Data from a Randomised Placebo Controlled Trial of Lamotrigine." *Journal of Neurology* 259, no. 3 (March 2012): 505–14. https://doi.org/10.1007/s00415-011-6212-9.

[64] Rocca, Maria A, Giovanna Mastronardo, Mariemma Rodegher, Giancarlo Comi, and Massimo Filippi. "Long-Term Changes of Magnetization Transfer-Derived Measures from Patients with Relapsing-Remitting and Secondary Progressive Multiple Sclerosis," *AJNR Am J Neuroradiol* 20 (1999):821–827

[65] Weiskopf, Nikolaus, Siawoosh Mohammadi, Antoine Lutti, and Martina F. Callaghan. "Advances in MRI-Based Computational Neuroanatomy: From Morphometry to in-Vivo Histology." *Current Opinion in Neurology* 28, no. 4 (August 2015): 313–22. https://doi.org/10.1097/WCO.0000000000000222.

[66] Hametner, Simon, Verena Endmayr, Andreas Deistung, Pilar Palmrich, Max Prihoda, Evelin Haimburger, Christian Menard, et al. "The Influence of Brain Iron and Myelin on Magnetic Susceptibility and Effective Transverse Relaxation - A Biochemical and Histological Validation Study." *NeuroImage* 179 (October 2018): 117–33. https://doi.org/10.1016/j.neuroimage.2018.06.007.

[67] Mangeat, G., S.T. Govindarajan, C. Mainero, and J. Cohen-Adad. "Multivariate Combination of Magnetization Transfer, T 2 * and B0 Orientation to Study the Myelo-Architecture of the in Vivo Human Cortex." *NeuroImage* 119 (October 2015): 89–102. https://doi.org/10.1016/j.neuroimage.2015.06.033.

[68] Dutta, R., and B. D. Trapp. "Pathogenesis of Axonal and Neuronal Damage in Multiple Sclerosis." *Neurology* 68, no. Issue 22, Supplement 3 (May 29, 2007): S22–31. https://doi.org/10.1212/01.wnl.0000275229.13012.32.

[69] Frischer, Josa M., Stephen D. Weigand, Yong Guo, Nilufer Kale, Joseph E. Parisi, Istvan Pirko, Jay Mandrekar, et al. "Clinical and Pathological Insights into the Dynamic Nature of the White Matter Multiple Sclerosis Plaque: Dynamic Nature of MS Plaque." *Annals of Neurology* 78, no. 5 (November 2015): 710–21. https://doi.org/10.1002/ana.24497.

[70] Lassmann, Hans, Wolfgang Brück, and Claudia Lucchinetti. "Heterogeneity of Multiple Sclerosis Pathogenesis: Implications for Diagnosis and Therapy." *Trends in Molecular Medicine* 7, no. 3 (March 2001): 115–21. https://doi.org/10.1016/S1471-4914(00)01909-2.

[71] Lucchinetti, Claudia, Wolfgang Brück, Joseph Parisi, Bernd Scheithauer, Moses Rodriguez, and Hans Lassmann. "Heterogeneity of Multiple Sclerosis Lesions: Implications for the Pathogenesis of Demyelination." *Annals of Neurology* 47, no. 6 (June 2000): 707–17. https://doi.org/10.1002/1531-8249(200006)47:6<707::AID-ANA3>3.0.CO;2-Q.

[72] Dousset, Vincent, Annick Gayou, Bruno Brochet, and Jean-Marie Caille. "Early Structural Changes in Acute MS Lesions Assessed by Serial Magnetization Transfer

Studies." *Neurology* 51, no. 4 (October 1998): 1150–55. https://doi.org/10.1212/WNL.51.4.1150.

[73] Levesque, Ives R., Paul S. Giacomini, Sridar Narayanan, Luciana T. Ribeiro, John G. Sled, Doug L. Arnold, and G. Bruce Pike. "Quantitative Magnetization Transfer and Myelin Water Imaging of the Evolution of Acute Multiple Sclerosis Lesions: Quantitative MT and T_2 in Acute MS Lesions." *Magnetic Resonance in Medicine* 63, no. 3 (March 2010): 633–40. https://doi.org/10.1002/mrm.22244.

[74] Elskamp, Ij van den, Dl Knol, H. Vrenken, G. Karas, A. Meijerman, M. Filippi, L. Kappos, et al. "Lesional Magnetization Transfer Ratio: A Feasible Outcome for Remyelinating Treatment Trials in Multiple Sclerosis." *Multiple Sclerosis Journal* 16, no. 6 (June 2010): 660–69. https://doi.org/10.1177/1352458510364630.

[75] Filippi, Massimo, Maria A. Rocca, Gianvito Martino, Mark A. Horsfield, and Giancarlo Comi. "Magnetization Transfer Changes in the Normal Appering White Matter Precede the Appearance of Enhancing Lesions in Patients with Multiple Sclerosis." *Annals of Neurology* 43, no. 6 (June 1998): 809–14. https://doi.org/10.1002/ana.410430616.

[76] Fazekas, F, S Ropele, C Enzinger, T Seifert, and S Strasser-Fuchs. "Quantitative Magnetization Transfer Imaging of Pre-Lesional White-Matter Changes in Multiple Sclerosis." *Multiple Sclerosis Journal* 8, no. 6 (December 2002): 479–84. https://doi.org/10.1191/1352458502ms860oa.

[77] Zheng, Yufan, Jar-Chi Lee, Richard Rudick, and Elizabeth Fisher. "Long-Term Magnetization Transfer Ratio Evolution in Multiple Sclerosis White Matter Lesions: Long-Term MTR Evolution in MS WM Lesions." *Journal of Neuroimaging* 28, no. 2 (March 2018): 191–98. https://doi.org/10.1111/jon.12480.

[78] Chawla, Sanjeev, Ilya Kister, Tim Sinnecker, Jens Wuerfel, Jean-Christophe Brisset, Friedemann Paul, and Yulin Ge. "Longitudinal Study of Multiple Sclerosis Lesions Using Ultra-High Field (7T) Multiparametric MR Imaging." Edited by Quan Jiang. *PLOS ONE* 13, no. 9 (September 13, 2018): e0202918. https://doi.org/10.1371/journal.pone.0202918.

[79] Lieury, Alice, Marie Chanal, Géraldine Androdias, Richard Reynolds, Sylvie Cavagna, Pascale Giraudon, Christian Confavreux, and Serge Nataf. "Tissue Remodeling in Periplaque Regions of Multiple Sclerosis Spinal Cord Lesions: Glia Remodeling in MS Spinal Cord." *Glia* 62, no. 10 (October 2014): 1645–58. https://doi.org/10.1002/glia.22705.

[80] Kuhlmann, Tanja, Samuel Ludwin, Alexandre Prat, Jack Antel, Wolfgang Brück, and Hans Lassmann. "An Updated Histological Classification System for Multiple Sclerosis Lesions." *Acta Neuropathologica* 133, no. 1 (January 2017): 13–24. https://doi.org/10.1007/s00401-016-1653-y.

[81] Lassmann, Hans, Wolfgang Brück, and Claudia F. Lucchinetti. "The Immunopathology of Multiple Sclerosis: An Overview." *Brain Pathology* 17, no. 2 (April 2007): 210–18. https://doi.org/10.1111/j.1750-3639.2007.00064.x.

[82] Dal-Bianco, Assunta, Günther Grabner, Claudia Kronnerwetter, Michael Weber, Romana Höftberger, Thomas Berger, Eduard Auff, et al. "Slow Expansion of Multiple Sclerosis Iron Rim Lesions: Pathology and 7 T Magnetic Resonance Imaging." *Acta Neuropathologica* 133, no. 1 (January 2017): 25–42. https://doi.org/10.1007/s00401-016-1636-z.

[83] Elliott, Colm, Jerry S Wolinsky, Stephen L Hauser, Ludwig Kappos, Frederik Barkhof, Corrado Bernasconi, Wei Wei, Shibeshih Belachew, and Douglas L Arnold. "Slowly Expanding/Evolving Lesions as a Magnetic Resonance Imaging Marker of Chronic Active Multiple Sclerosis Lesions." *Multiple Sclerosis Journal* 25, no. 14 (December 2019): 1915–25. https://doi.org/10.1177/1352458518814117.

[84] De Stefano, N., A. Giorgio, M. Battaglini, M. Rovaris, M. P. Sormani, F. Barkhof, T. Korteweg, et al. "Assessing Brain Atrophy Rates in a Large Population of Untreated Multiple Sclerosis Subtypes." *Neurology* 74, no. 23 (June 8, 2010): 1868–76. https://doi.org/10.1212/WNL.0b013e3181e24136.

[85] Eshaghi, Arman, Ferran Prados, Wallace J. Brownlee, Daniel R. Altmann, Carmen Tur, M. Jorge Cardoso, Floriana De Angelis, et al. "Deep Gray Matter Volume Loss Drives

963 Disability Worsening in Multiple Sclerosis: Deep Gray Matter Volume Loss." *Annals of*
964 *Neurology* 83, no. 2 (February 2018): 210–22. https://doi.org/10.1002/ana.25145.
965
966 [86] Bermel, Robert A, and Rohit Bakshi. "The Measurement and Clinical Relevance of
967 Brain Atrophy in Multiple Sclerosis." *The Lancet Neurology* 5, no. 2 (February 2006):
968 158–70. https://doi.org/10.1016/S1474-4422(06)70349-0.
969
970 [87] Zivadinov, R., A. T. Reder, M. Filippi, A. Minagar, O. Stuve, H. Lassmann, M. K.
971 Racke, M. G. Dwyer, E. M. Frohman, and O. Khan. "Mechanisms of Action of Disease-
972 Modifying Agents and Brain Volume Changes in Multiple Sclerosis." *Neurology* 71, no.
973 2 (July 8, 2008): 136–44. https://doi.org/10.1212/01.wnl.0000316810.01120.05.
974
975 [88] De Stefano, Nicola, Maria Laura Stromillo, Antonio Giorgio, Maria Letizia Bartolozzi,
976 Marco Battaglini, Mariella Baldini, Emilio Portaccio, Maria Pia Amato, and Maria Pia
977 Sormani. "Establishing Pathological Cut-Offs of Brain Atrophy Rates in Multiple
978 Sclerosis." *Journal of Neurology, Neurosurgery & Psychiatry*, April 22, 2015, jnnp-2014-
979 309903. https://doi.org/10.1136/jnnp-2014-309903.
980
981 [89] on behalf of the MAGNIMS study group, Christian Enzinger, Frederik Barkhof, Olga
982 Ciccarelli, Massimo Filippi, Ludwig Kappos, Maria A. Rocca, et al. "Nonconventional MRI
983 and Microstructural Cerebral Changes in Multiple Sclerosis." *Nature Reviews Neurology*
984 11, no. 12 (December 2015): 676–86. https://doi.org/10.1038/nrneurol.2015.194.
985

[90] Bodini, Benedetta, Mattia Veronese, Daniel García-Lorenzo, Marco Battaglini, Emilie Poirion, Audrey Chardain, Léorah Freeman, et al. "Dynamic Imaging of Individual Remyelination Profiles in Multiple Sclerosis." *Annals of Neurology* 79, no. 5 (May 2016): 726–38. https://doi.org/10.1002/ana.24620.

[91] Patrikios, P., C. Stadelmann, A. Kutzelnigg, H. Rauschka, M. Schmidbauer, H. Laursen, P. S. Sorensen, W. Bruck, C. Lucchinetti, and H. Lassmann. "Remyelination Is Extensive in a Subset of Multiple Sclerosis Patients." *Brain* 129, no. 12 (June 9, 2006): 3165–72. https://doi.org/10.1093/brain/awl217.